Carbohydrate Polymers 347 (2025) 122733

Contents lists available at ScienceDirect

Carbohydrate Polymers

journal homepage: www.elsevier.com/locate/carbpol

Effect of alkali treatment and fungal degradation on the nanostructure and cellulose arrangement in Scots pine cell walls – A neutron and X-ray scattering study

Magdalena Broda [a,*], Nayomi Z. Plaza [b,*], Joseph E. Jakes [b], Carlos Baez [b], Sai Venkatesh Pingali [c], Wim Bras [d]

[a] Department of Wood Science and Thermal Techniques, Faculty of Forestry and Wood Technology, Poznan University of Life Sciences, ul. Wojska Polskiego 38/42, 60-637 Poznan, Poland
[b] Forest Products Laboratory, Forest Service, United States Department of Agriculture, Madison, WI 53726, USA
[c] Neutron Scattering Division, Oak Ridge National Laboratory, Oak Ridge, TN 37831, USA
[d] Chemical Sciences Division, Oak Ridge National Laboratory, Oak Ridge, TN 37831, USA

ARTICLE INFO

Keywords:
Wood degradation
Cell wall nanostructure
Neutron scattering
Cellulose microfibrils
Cellulose arrangement
Cellulose crystallinity

ABSTRACT

Research on new conservation treatments for historical wood requires considerable amounts of appropriate wood material, which is hard to acquire. Thus, we produced biologically and chemically degraded model wood that could be used as a representative material in future research on consolidating agents. Using chemical composition determinations, we found that fungal decay targeted mainly polysaccharides, while alkaline treatment mostly reduced hemicelluloses and lignin content. X-ray and neutron scattering showed that all decayed samples had increased disorder in microfibril alignment and larger elementary fibril cross-sections, and alkaline-treated samples had much larger elementary fibril spacing compared to those decayed by fungi. These nanoscale and chemical differences correlate with physical property changes. For example, decreased cellulose crystallinity and increased disorder of the microfibrils in degraded cell walls likely contribute to the lower elastic moduli measured for these cell walls. The obtained data improves understanding of how degradation alters wood structures and properties across length scales and will be valuable for future studies focusing on archeological wood. Moreover, it leads to the conclusion that it is more appropriate to develop treatments that consider not only spatial variability and degree of wood degradation but also the corresponding molecular and nanoscale changes in the cell walls.

1. Introduction

Wood degradation is essential to global carbon cycling. It is caused mainly by fungal decay, but several other abiotic and biotic factors also play an important role, including UV radiation, precipitation, temperature changes, mechanical forces (wind), and microbial or insect activity (Arpaci et al., 2021; Brischke & Alfredsen, 2020). The weathering of wood limits its broader use, particularly in outdoor applications. Therefore, significant effort has been invested in improving wood performance using various treatments and design solutions (Hill et al., 2022; Sandberg et al., 2017; Spear et al., 2021).

While degradation processes are harmful to wood in service, they also affect valuable historical wooden artifacts excavated from wet soil or water bodies, necessitating a search for effective and reliable conservation methods to preserve what has been left and prevent further degradation (Aluri et al., 2020; Broda & Hill, 2021; Monaco et al., 2018; Zisi, 2021). However, extensive research on new conservation agents requires large amounts of material. Moreover, studying the properties of historical wood often employs destructive analytical techniques, which leads to the loss of the examined material. Therefore, to avoid the unacceptable loss of priceless wooden objects for these purposes, researchers can use artificial degradation processes to produce model material that can mimic naturally decayed historical wood (Albelda Berenguer et al., 2019; Broda & Plaza, 2023; Franceschi et al., 2008; Kennedy & Pennington, 2014; Liu et al., 2019; Tahira et al., 2017; Wakefield et al., 2020).

* Corresponding authors.
E-mail addresses: magdalena.broda@up.poznan.pl (M. Broda), nayomi.plazarodriguez@usda.gov (N.Z. Plaza).

https://doi.org/10.1016/j.carbpol.2024.122733
Received 20 May 2024; Received in revised form 5 September 2024; Accepted 8 September 2024
Available online 12 September 2024

Existing conservation methods for waterlogged archeological wood are not entirely reliable or efficient (Broda & Hill, 2021). To address this, we are researching organosilicon compounds as a potential alternative to the currently used conservation methods (Broda, Mazela, & Dutkiewicz, 2019; Broda, Mazela, & Radka, 2019). However, the research requires large quantities of similar wood samples to test the effectiveness of different organosilicon compound conservation treatments. Since obtaining enough amounts of naturally and evenly degraded waterlogged archeological wood material for the study was difficult, we decided to produce degraded model wood samples employing biotic decay by the brown-rot fungus *Coniophora puteana* (Shum.: Fr.) P. Karst and chemical degradation using an alkaline treatment with 50 % NaOH (Broda, Popescu, et al., 2022).

Biotic wood degradation is a natural process that depends on oxygen availability, moisture content, and temperature. In terrestrial environments, it is primarily caused by brown-, white- and soft-rot wood-decaying fungi that decompose mainly wood polysaccharides but can also degrade (white-rot) or modify (brown-rot) lignin (Goodell et al., 2008; Pournou, 2020b). In aquatic environments, wood degradation by soft-rot and anaerobic or facultative anaerobic bacteria predominate, depriving the cell wall of carbohydrates and partially lignin (tunneling bacteria) (Blanchette, 2000; Pournou, 2020a). The choice of using *C. puteana* for the degradation of model wood was dictated by its high effectiveness in decaying softwood (pine was chosen as a model material), easiness in cultivation under laboratory conditions, commonality in use in wood mycological tests, and the fact that it degrades mainly cell wall polysaccharides, similarly to microorganisms that decompose wood under waterlogged/saturated conditions (Bagley & Richter, 2002; Brischke et al., 2020).

Alkaline hydrolysis is used to delignify wood and other lignocellulosic biomass in pulp and paper production, modify the surface, and enhance the tensile strength of natural fibers (Cai et al., 2015; Crawshaw et al., 2002; Dai & Fan, 2014; Larocque & Maass, 1941; Raia et al., 2021; Wei et al., 2018). NaOH solution can effectively degrade lignin, even up to 95 % of its content in wood. However, the process is not fully selective and also leads to the decomposition of hemicelluloses. Higher sodium hydroxide concentrations may even cause the cellulose to transform from the native type I to type II (Bakri et al., 2016; Nishiyama et al., 2000; Raia et al., 2021; E. Xu et al., 2020). Wood degraded with an alkali solution has already been used as a model material in several studies on new conservation treatments (Kennedy & Pennington, 2014; Liu et al., 2019; Tahira et al., 2017), hence the idea to employ this method in our research, too. Moreover, since chemically degraded wood is abundant with cellulose, the nutrient source for fungi, this model wood should also be a good material for studying the potential antifungal effectiveness of the organosilicon treatment, which is an important subsidiary role of an effective wood consolidation agent.

Although there are several studies on changes in the wood chemical composition, structure, and properties due to fungal decay (Bagley & Richter, 2002; Bari et al., 2020; Brischke et al., 2019; Curling et al., 2002; Goodell et al., 2020; Pandey & Pitman, 2003; Zabel & Morrell, 2020; Zhu et al., 2020) and alkaline hydrolysis (Bakri et al., 2016; S. Y. Chen et al., 2018; Ishikura et al., 2010; Ishikura & Nakano, 2005, 2007; Saiful Islam et al., 2012; E. Xu et al., 2020), the effects of degradation on the cell wall nanostructure are still not entirely recognized. Furthermore, we know that some organosilicon molecules we plan to use as wood consolidants in future research are in the nano-size, and they can infiltrate and alter the cell wall structure (Broda et al., 2023, 2024). Therefore, we decided to use experimental techniques that can provide more insights into structural changes over the 0.1–100 nm range, namely, small-angle neutron scattering (SANS) as well as small- and wide-angle X-ray scattering (SAXS and WAXS). SANS, SAXS, and WAXS have proven to be particularly useful for research on the hierarchical structure of plant cell walls on the nanoscale (Martínez-Sanz et al., 2015; Penttilä, Altgen, Awais, et al., 2020), interactions of water with the nanoscale components of the wood cell wall and the resulting moisture-induced structural changes (Penttilä et al., 2021; Penttilä, Altgen, Carl, et al., 2020; Plaza et al., 2016; Plaza et al., 2018; Zitting et al., 2021), and the effect of various wood modifications and treatments on the cell wall nanostructure (P. Chen et al., 2021; Guo et al., 2016; Ibach et al., 2022; Plaza et al., 2022; Toba et al., 2013). Thus, here, we used both X-ray and neutron techniques to elucidate different structural aspects of wood. The enhanced contrast achieved with neutrons allowed us to measure changes in the elementary fibril spacing, while X-rays, in this case, were more sensitive to the cellulose crystalline structure and microfibril alignment in the cell walls. Here, cellulose elementary fibrils are a universal structural unit of cellulose, whose cross-section is about 2–3 nm (Fernando et al., 2023; Jakob et al., 1995; P. Xu et al., 2007; Zhang et al., 1997), and aggregate into bundles called microfibrils (Heyn, 1969). By combining the neutron and X-ray scattering results with previously acquired data on the structural, moisture, and mechanical properties of model degraded wood, we have obtained a more complete view of how nanoscale changes are correlated with wood's structural integrity and strength, which might be affected much more rapidly by degradation, even before a considerable weight loss is observed. This knowledge is crucial for developing and improving methods to conserve historical wooden artifacts and better protect wood in service.

1.1. Hypothesis

Biologically and chemically degraded wood has different chemical composition and nanostructure, particularly at the elementary fibril level, compared to intact wood, which are contributing factors to their modified mechanical and moisture properties.

2. Materials and methods

2.1. Specimen preparation

Scots pine (*Pinus sylvestris* L.) wood purchased from commercial timber merchants in the Wielkopolska Region, Poland, was used in this research. Straight-grained, knot- and defect-free small blocks 20 mm (radial) x 20 mm (tangential) x 10 mm (longitudinal) in size were prepared from a single plank of sawn timber. To mimic degraded archeological wood, some samples were degraded chemically by soaking in 50 % NaOH for 3 weeks at room temperature, while others were degraded biologically by exposing for 8 weeks to the common wood-decaying brown-rot fungus *Coniophora puteana* (Shum.: Fr.) P. Karst BAM 112 (BAM Ebw. 15). Further details about the culture and method details can be found in (Broda, Popescu, et al., 2022)). After chemical and biological degradation, the average mass loss of samples was 17 $\pm$ 1 % and 39 $\pm$ 5 %, respectively. The degraded specimens were air-dried at 20 $\pm$ 3 °C and relative humidity of 45 $\pm$ 5 % and subjected to further testing. Sound Scots pine wood was used as a reference.

2.2. Wood chemical composition

A quantitative analysis of wood to measure total lignin and carbohydrate content was performed according to the NREL procedure (Sluiter et al., 2008). This method allows for fractionating wooden biomass into simpler forms that are easier to quantify. The measured components include acid-soluble lignin (measured by UV–Vis spectrometry), acid-insoluble lignin (that may include ash, measured gravimetrically), and hydrolyzed, soluble monomeric forms of wood carbohydrates measured using Ion chromatography. Approximately 40 mg of the sample was used for the measurement, and samples were analyzed in duplicate. For sugar analysis, a Dionex ICS 3000 HPLC system equipped with a pulsed amperometric detector configured to be sensitive to carbohydrates was used along with the Dionex CarboPac PA1 (4 $\times$ 250 mm) column. The mobile phase was water; additionally, 200 mM NaOH solution was added post-column to ionize the sugars and

increase detection sensitivity.

2.3. Small-angle neutron scattering (SANS)

Wood blocks were soaked in water and then cut perpendicularly against the growth rings to reveal a smooth radial-longitudinal surface. Then, sections approximately 0.7 mm thick were cut from the exposed surface. These sections were air-dried at room temperature under a fume hood for over 24 h prior to the experiments. The thin specimens were soaked in D_2O overnight and then placed inside titanium holders with a 1 mm spacer. Air bubbles were removed, and the cells were re-filled with D_2O as needed. SANS measurements were performed with the Bio-SANS instrument at the High Flux Isotope Reactor facility at the Oak Ridge National Laboratory (Heller et al., 2014). To achieve a broad dynamic range ($0.003 < q < 0.85$ Å^{-1}), we used an incident wavelength of 6 Å and a dual-detector configuration consisting of the main detector at 15.5 m and a curved wing detector fixed at 1.13 m from the sample and rotated at 1.4°. Two-dimensional detector patterns were corrected for background, pixel sensitivity, dark current, and solid angle and normalized by monitor counts. To measure the average wood nanostructure, a large spot size (14 mm) was used to probe many wood cells simultaneously.

Data was anisotropically reduced using a reduction package developed by ORNL (Heller et al., 2022). The equatorial scattering data $I(q)$ was modeled in IRENA (Ilavsky & Jemian, 2009) using the following equation:

$$I(q) = B_1 q^{-P_1} + B_2 q^{-P_2} + A e^{\frac{(q-q_0)^2}{w^2}} + B_3 \quad (1)$$

where P_1 and P_2 are the power law exponents, B_1 and B_2 are the power law prefactors, and B_3 is the background. The third term corresponds to the Gaussian diffraction peak described in terms of its amplitude A, peak position (q_0), and width (w). Then, the distance between the elementary fibrils (EF_s) was determined from the peak position as follows: $EF_s = 2\pi/q_0$. Initially, all parameters were allowed to vary, and then the low-q power law exponent (P_1) was fixed to four since it was similar for all samples. So, there were a total of seven free parameters (B_1, P_2, B_2, A, w, q_0, and B_3) in the final fit. Additionally, we evaluated the relationship between the determined peak position and the peak width (w) by fixing the peak width to three different values and calculating the corresponding EF_s from the fitted peak position.

2.4. Wide-angle X-ray scattering and small-angle X-ray scattering (WAXS/SAXS)

Thin specimens (~0.7 mm thick) were prepared following the same procedure outlined previously for SANS. Structural characterization spanning from 0.0035 to 3.4 Å^{-1} was conducted using a Xeuss 3.0 by Xenocs (Grenoble, France) X-ray scattering system equipped with a Ga metal jet source (9.2 keV) and an Eiger Dectris 2D detector array. The transmission geometry was used for all samples with a sample-to-detector distance of 900 mm and 55 mm for SAXS and WAXS measurements, respectively. All samples were taped onto a flat plate holder, and each sample was exposed for 300 s using a 0.5 mm spot size so that the scattering volume being probed included many wood cells. All measurements were performed under a vacuum to reduce air scattering contributions. The data was both anisotropically and azimuthally integrated using NIKA (Ilavsky, 2012) and a custom Python script using the Fabio library (Knudsen et al., 2013). The scattering profiles were corrected for background contributions, and the equatorial data was fitted.

The SAXS data was fitted to the WoodSAS model (Penttilä et al., 2019) simultaneously with meridionally subtracted SANS data to determine if observed trends are affected by variations in the analysis approach.

$$I(q) = Cq^{-4} + B\exp\left(-\frac{q^2}{2\sigma^2}\right) + DI_{cyl}(q, \overline{R}, \Delta R = 0.2, a, \Delta a = 0.35) \quad (2)$$

Here, C, B, and D, are scalars. The first term describes the low-q power law scattering with an exponent of four, the second term is a broad Gaussian peak centered at $q = 0$, and its width (σ) has been used to calculate the microfibril bundle width (B_w) as follows: $B_w = \frac{2\sqrt{2}}{\sigma}$ (Penttilä, Altgen, Awais, et al., 2020). The third term (I_{cyl} function) describes the high-q as the scattering from an array of infinitely long cylinders whose radius follow a Gaussian distribution with mean $\overline{R}$ and standard deviation ΔR, and are arranged in a hexagonal lattice with a spacing (a) and paracrystalline distortion (Δa). To improve the fit and reduce the number of free parameters, the polydispersity parameters were fixed during the fitting to $\Delta R = 0.2$ and $\Delta a = 0.35$, and $\overline{R}$ was constrained to be the same for SAXS/SANS curves. Considering that SANS and SAXS yield different radii as discussed in the supplementary section in Chen et al., 2021 (*P.* Chen et al., 2021), and that the fit results are more weighted to the SANS data, the obtained $\overline{R}$ would correspond to the crystalline region of the elementary fibril cross-section and this value will be smaller than the real elementary fibril radius. Parameters were fit sequentially (a then $\overline{R}$), and only allowed to vary within reason due to the known overlap in the form factor and structure factor contributions, also described in the supplementary information section of Chen et al., 2021 (*P.* Chen et al., 2021).

The WAXS data was modeled using a Pseudo-Voigt peak for each diffraction typically observed for cellulose Iβ, namely, the 200, the 004, the doublets (110 and 1–10). The 020 peak was also included to improve the overall fit. Additionally, the azimuthal spread from the SAXS and WAXS datasets was evaluated to determine the degradation effects on the microfibril angle (MFA). To obtain the MFA, the azimuthal scattering profiles were fitted following Lichtenegger et al. (H. C. Lichtenegger et al., 2001) with one or three Gaussian peaks for the intact and chemically degraded samples and two Gaussian peaks for the biologically degraded sample due to the splitting observed in the azimuthal profile.

2.5. Microscopy

Microscopy was used to examine the cross-sectional shape of tracheids and the integrity of wood cell walls. The microscopy was obtained from wood surfaces prepared for nanoindentation using a diamond knife, as previously described (Broda et al., 2024). Optical microscopy images were collected using the optical microscope incorporated into the Bruker-Hysitron (Minneapolis, Minnesota, USA) TriboIndenter. The scanning probe microscopy (SPM) images were obtained using the TriboIndenter by raster scanning a Berkovich probe over the cell walls.

3. Results

To understand the effects of two different degradation processes on the nanostructure of the pinewood cell wall, we analyzed the chemical composition of the cell walls and investigated the effect of the degradation on the nanostructure with neutron and X-ray scattering techniques.

The chemical composition of degraded pinewood differed from the intact one (Table 1). Fungal exposure to *C. puteana* (BP) reduced the xylan and mannan contents by 33 % and 48 %, respectively. BP had approximately 13 % less holocellulose and more lignin than intact wood (CP). Extensive loss of hemicelluloses, the most accessible nutrient source in wood cell walls (Ringman et al., 2014; Rowell et al., 2009), was also evident by the concurrent decrease in pentosane content (37 % less) and relative increase in the Glu/Xyl and Glu/Man ratios observed in BP. These changes in cell wall chemical composition are characteristic

Table 1
Chemical composition of undegraded (CP), biologically (BP), and chemically (ChP) degraded pine wood ± standard deviation; AIL – acid-insoluble lignin, ASL – acid-soluble lignin, Arab – arabinan, Galact – galactan, Gluc – glucan, Xyl – xylan, Man – mannan, L – total lignin. Holocelluloses (H, all sugars) and pentosanes (arabinan and xylan) were calculated as total content per yield. Sample composition is reported as weight percent on an oven-dry weight basis.

Sample ID	Sample composition (%)								Yield		H	Pentosanes	Glu/Xyl	Glu/Man
	AIL	ASL	L	Ash	Arab	Galact	Gluc	Xyl	Man	(%)	(%)	(%)		
CP	30.9 ± 0.1	3.0 ± 0.1	33.9 ± 0.1	0.9 ± 0.2	1.40 ± 0.1	1.3 ± 0.03	38.1 ± 0.8	5.2 ± 0.3	10.2 ± 0.1	90.9 ± 0.8	61.8 ± 0.9	7.2 ± 0.4	7.4 ± 0.4	3.7 ± 0.1
BP	36.2 ± 0.4	4.5 ± 0.5	40.7 ± 0.1	0.8 ± 0.1	0.78 ± 0.02	0.6 ± 0.02	38.6 ± 0.7	3.5 ± 0.1	5.4 ± 0.1	90.2 ± 0.9	54.1 ± 0.8	4.7 ± 0.1	11.2 ± 0.1	7.2 ± 0.1
ChP	31.6 ± 0.2	2.3 ± 0.1	33.9 ± 0.2	0.6 ± 0.2	0.99 ± 0.02	1.1 ± 0.03	41.2 ± 0.7	4.0 ± 0.1	12.9 ± 0.3	94.7 ± 1.1	63.5 ± 0.6	5.3 ± 0.1	10.3 ± 0.1	3.2 ± 0.03

of wood degradation by brown-rot fungi (Li et al., 2011; Pandey & Pitman, 2003). Treatment with sodium hydroxide (ChP) also removed some hemicelluloses but to a lesser extent, as evidenced by the increased Glu/Xyl and 27 % lower pentosane content. Despite having similar lignin and holocellulose content to undegraded pine, ChP had approximately 20 % less acid-soluble lignin and 22 % less xylan. These results indicate that the treatment removed and/or degraded some lignin and hemicelluloses, which is characteristic of alkaline hydrolysis with NaOH solutions (Bakri et al., 2016; Raia et al., 2021; E. Xu et al., 2020).

The effects of different types of degradation on small-angle neutron scattering (SANS) from pine immersed in heavy water are shown in Fig. 1. Here, the contrast between water-accessible regions and non-water-accessible regions within the cell wall can allow us to detect nanoscale changes in wood nanostructure. CP samples showed strong anisotropic scattering, and the long-range order of the cellulose elementary fibrils resulted in a diffraction peak observed both in the 2D pattern (Fig. 1 d) and the equatorial scattering profile in Fig. 1g. For degraded samples, scattering patterns were still anisotropic but more diffuse, and the diffraction peaks were not as pronounced. For the wet BP sample, the diffraction peak had decreased height, was broader, and the position shifted from 0.146 to 0.129 $Å^{-1}$. This indicates that the long-range order was reduced, and the distance between the cellulose elementary fibrils was larger and more polydisperse. For the wet ChP sample, the diffraction peak was broader and shifted to considerably lower q (0.076 $Å^{-1}$ compared to 0.146 $Å^{-1}$ for CP). This indicates that the spacing between the cellulose elementary fibrils was not only more polydisperse but also larger in the ChP sample compared to the other samples.

By fitting the equatorial scattering to an empirical model (Eq. 1), we were able to quantify changes caused by degradation in terms of the following parameters: *mid-q* power law slope (P_2), prefactor (B_2), the cellulose elementary fibril spacing (EF_s) and amplitude of the small angle diffraction peak (A) (Table 2).

The EF_s is the center-to-center distance between neighboring cellulose elementary fibrils. In the low regime ($q < 0.01\ Å^{-1}$), the scattering was dominated by larger structures, and we observed power law scattering with an exponent of 4 for all samples, which was then fixed during subsequent fitting. Scattering from all wood polymers can contribute to the *mid-q* region, as well as some minor contributions from the tails of the *high* and *low q* scattering regions; thus, determining what gives rise to the scattering in this region can be difficult. For the intact sample, P_2 was 1 (which corresponds to scattering from rod-like structures); during the uncertainty analysis, this value was fixed to reduce the number of free parameters. Both types of degradation had a slight increase in P_2 compared to CP, and the exponents obtained were similar to those observed for wood treated with low levels of alkylene oxides (Ibach et al., 2022). In the *high-q*, the elementary fibril spacing (EF_s) increased most significantly for the chemically degraded sample. Conversely, for the BP sample, the *high-q* peak was less intense, and the corresponding EFs had a slightly higher value but also higher uncertainty than CP.

Degraded samples had less intense and broader small-angle diffraction peaks. Hence, the fitted peak position varied depending on the peak width (Table 3). In general, we observed that increasing the peak width led to higher spacings with larger uncertainties, which was most noticeable in the degraded samples. Nevertheless, EF_s was always 3–6 nm higher for ChP than CP or BP samples.

The effects of degradation on the X-ray scattering data for dry samples measured in vacuum were less pronounced (Fig. 2) compared to the SANS data. However, by comparing the equatorial scattering patterns, we observed that the most pronounced differences were visible in the SAXS regime ($q < 0.5\ Å^{-1}$). In the WAXS region ($q > 0.5\ Å^{-1}$), the differences between samples were more subtle, and the cellulose Iβ characteristic diffraction peaks were still present in all samples. This suggests that while much of the cellulose crystalline structure is unaltered, the long-range order and aggregation of the cellulose elementary fibrils were affected by the degradation mechanisms. In general, the

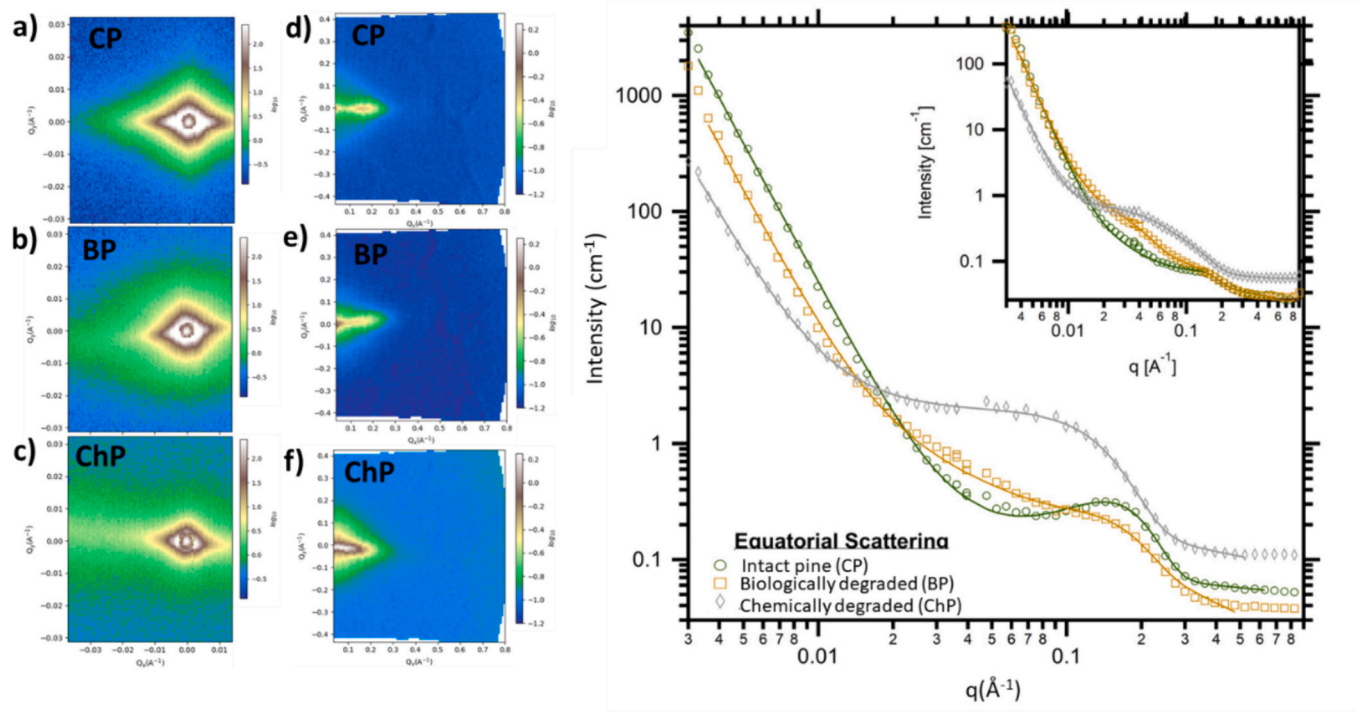

Fig. 1. Effects on degradation on SANS data from pine samples immersed in heavy water. (a-c) Small angle and (d-f) wide angle detector data for pine. Data from (a, d) intact pine (CP), (b, e) biologically degraded pine (BP), and (c, f) chemically degraded pine (ChP). (g) Integrated scattering profiles from the equatorial sectors (strongly aligned scattering regions). Meridional scattering profiles are shown in the inset. Overlaid lines correspond to fits to the scattering data. All degraded samples show a clear shift in the peak towards lower *q*, which indicates that the elementary fibril spacing is increasing.

Table 2
Effects of the degradation process on the SANS scattering parameters from eq. 1 for undegraded (CP), biologically degraded (BP), and chemically degraded (ChP) pine wood. Uncertainties are included in parenthesis. Parameters marked with an asterisk (*) were held fixed during the uncertainty analysis. The *low-q* power law exponent was fixed at 4 and the *high-q* peak width (w) was fixed at 0.06 $Å^{-1}$ for all.

Sample ID	Mid-q ($0.01\ Å^{-1} < q < \sim 0.1\ Å^{-1}$)		High-q ($q > \sim 0.1\ Å^{-1}$)	
	B_2	P	EF_s (nm)	A
CP	0.006 (0.003)	1*	4.3 (0.2)	0.22 (0.03)
BP	0.006 (0.003)	1.2 (0.1)	4.9 (0.5)	0.13 (0.03)
ChP	0.0084 (0.004)	1.2 (0.1)	8.3 (0.4)	1.4 (0.1)

Table 3
Dependence of the elementary fibril spacing (EF_s) on the fixed peak width (w) for undegraded (CP), biologically degraded (BP), and chemically degraded (ChP) pine wood samples. Fit uncertainties are included in parenthesis.

	EF_s (nm)		
Sample ID	0.06 ($Å^{-1}$)	0.07 ($Å^{-1}$)	0.08 ($Å^{-1}$)
CP	4.3 (0.2)	4.4 (0.2)	4.7 (0.3)
BP	4.9 (0.5)	5.0 (0.5)	5.5 (0.6)
ChP	8.3 (0.4)	8.7 (0.4)	10.7 (0.5)

SAXS shoulder shifted from ~0.15 $Å^{-1}$ to ~0.08 $Å^{-1}$ in the degraded samples, especially for the ChP sample, which is consistent with the SANS data.

Results obtained from fitting the SAXS and SANS data using the WoodSAS model (Eq. 2) are listed in Table 4. Overall trends in the elementary fibril spacing agree with the SANS analysis using eq. 1, and all degraded samples had larger spacings (*a*) in wet conditions. BP only had increased spacing when wet, meaning that this type of degradation allowed the microfibrils to swell more than CP. ChP had a higher elementary fibril spacing than CP in both dry and wet conditions, meaning that this type of degradation, which also had the largest EF_{dia}, increased both the cross-section of the elementary fibrils and the microfibril swelling compared to CP.

Though the mid-q bundle width has been previously attributed to microfibrils (typically between 10 and 20 nm for unmodified softwoods (Donaldson, 2007; Fahlén & Salmén, 2003; Penttilä, Altgen, Awais, et al., 2020), the values obtained are much smaller than expected (particularly for SAXS). This is likely indicating that retrieving the microfibril size from scattering data alone is not possible given the poor contrast between microfibrils, the lack of uniformity in the microfibril size (there is a large number of microfibrils that only have 3 to 4 elementary fibrils (Addison et al., 2024; Fernando et al., 2023; Kirui et al., 2022; P. Xu et al., 2007), and the large contribution of highly correlated elementary fibrils.

As expected, fitting the WAXS data revealed only minor variations in the spacing between the cellulose Iβ diffraction planes (Table 5). Overall, the spacing between the planes increased, which is consistent with previous observations attributed to the mercerization of cellulose and the formation of Na-cellulose IV (Nishimura et al., 1991), as well as the degradation of cellulose by brown rot (Goodell et al., 2017). These trends agree with the observed increases in the EF_{dia}. The largest changes were observed for the ChP sample, particularly in the doublet region (i.e., 110). It should be noted that for this sample, we also observed larger spacings between elementary fibrils in both dry and fully immersed conditions.

We also observed changes in the anisotropy of the scattering patterns between the different degradation processes (Fig. 3).

The anisotropic scattering features become less pronounced for both degradation methods. Given the orientation of the samples, we compared the azimuthal profiles to calculate the microfibril angle (MFA) of the cellulose microfibrils in the wood cell walls. Typically, for intact wood, this can be measured with either SAXS or WAXS. However, here, for the ChP sample, the microfibril angle measured from SAXS is larger

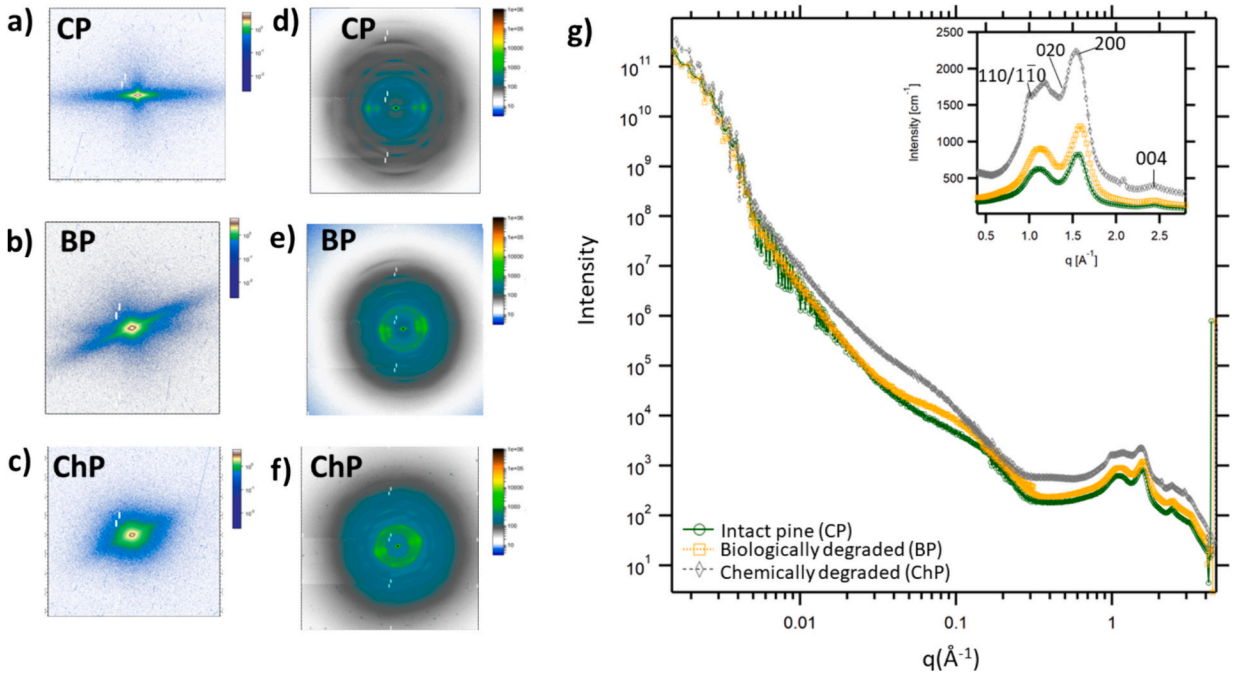

Fig. 2. Effects of degradation on x-ray scattering data from dry pine samples including intact pine (CP), biologically degraded pine (BP), and chemically degraded pine (ChP). All samples were measured under a vacuum to reduce air scattering. SAXS data (a-c) was obtained with a detector distance of 900 mm, and WAXS data (d-f) was obtained at 55 mm. (g) Equatorial scattering profiles showing both SAXS and WAXS regimes. The clear changes in the SAXS region are evidence of elementary fibrils that are more disordered and spaced further apart, especially for ChP, despite still having the characteristic cellulose Iβ diffraction peaks in the WAXS region (shown in the inset).

Table 4
Parameters obtained by fitting the SAXS equatorial data to the WoodSAS (Penttilä et al., 2019) model, where a is the spacing between elementary fibrils arranged in a hexagonal array. The elementary fibril size polydispersity was fixed (ΔR =0.2), and the lattice distortion parameter was fixed (Δa = 0.35) for undegraded (CP), biologically degraded (BP) and chemically degraded (ChP) pine wood samples. Uncertainties included in parenthesis correspond to values from the fitting algorithm in SASVIEW. ** This value corresponds to the maximum limit allowed in the fitting routine.

Sample ID	*Mid-q* Bundle width (nm)		*High-q*		
			a (nm)		EF_{dia} (nm)
	Dry (SAXS)	Wet (SANS)	Dry (SAXS)	Wet (SANS)	SAXS/ SANS
CP	3.39 (0.006)	28.3**	3.17 (0.3)	3.75 (0.2)	1.90 (0.03)
BP	4.1 (0.004)	7.0 (0.010)	3.15 (0.1)	4.30 (0.3)	1.97 (0.03)
ChP	5.8 (0.002)	28.3**	3.98 (0.2)	6.95 (0.2)	2.5 (0.07)

Table 5
Effects of degradation process on the WAXS diffraction peak positions for intact (CP), biologically degraded (BP), and chemically degraded (ChP) pine wood samples. Fit uncertainties are included in parenthesis.

Sample ID	d200 (Å)	d110 (Å)	d1–10 (Å)	d020 (Å)	d004 (Å)
CP	3.97 (0.03)	6.03 (0.05)	5.31 (0.06)	4.25 (0.03)	2.55 (0.02)
BP	4.03 (0.02)	6.04 (0.01)	5.20 (0.09)	4.44 (0.03)	2.56 (0.09)
ChP	4.05 (0.05)	6.36 (0.12)	5.31 (0.08)	4.58 (0.12)	2.58 (0.03)

than the one measured from WAXS, even though the scattering volume being probed is the same (Table 6).

This difference suggests that chemically degrading the samples introduces distortions and leads to a mismatch between the measured orientation of the semi-crystalline cellulose via WAXS and the larger length scales accessible via SAXS. It is also possible that there are some nanoscale features formed due to the degradation process that contribute to the SAXS regime, such as residues or pores (Broda, Popescu, et al., 2022). Such features would probably be isotropic and mostly contribute to the background of the SAXS signal. Further research on this area could help explain the observed differences. The splitting of the peak observed in the BP sample was accounted for in the determination of the MFA, and it is likely caused by the orientation of the cell walls with respect to the beam. Similar results have been observed previously when the perpendicular plane of the irradiated wood cell walls has some rotation with respect to the radial plane (Entwistle et al., 2005; H. Lichtenegger et al., 1999). It should be noted that MFA can vary considerably even for normal wood, and in this study, the MFA of the individual sapwood blocks was not measured prior to the artificial degradation. Nevertheless, degraded samples had a larger MFA compared to the intact wood (Table 6), which is consistent with previous observations of increased MFA in fungal-decayed historic sapwood (Hudson-McAulay et al., 2018) via x-ray diffraction.

From scanning probe microscopy images and optical microscopy images of prepared nanoindentation surfaces (Figs. 4A and B), the difference in the shape of cell lumina between ChP and the rest of the examined wood types can be seen. The lumina in ChP are misshapen, smaller, and often diamond-shaped (ChP in Fig. 4B), as if the cell walls of ChP were pushed into the lumina. It may be caused by swelling forces during treatment, which possibly have arisen from the increase in spacing of the cellulose lattice caused by Na ions (Cai et al., 2015; Nishiyama et al., 2000; Raia et al., 2021). The literature data suggest that the alkaline treatment leads to breaking and re-arranging hydrogen bonds, which results in fiber swell and fibrillation that increases the effective surface area and the number of free hydroxy groups available for interactions with water (Broda, Popescu, et al., 2022; Cai et al., 2015; Dai & Fan, 2014). Despite the changes caused by alkaline treatment, the S2 layers in the ChP samples retained integrity similarly to CP and BP samples, as can be seen in the scanning probe microscopy images (ChP in Fig. 4A vs. CP and BP in Fig. 4A).

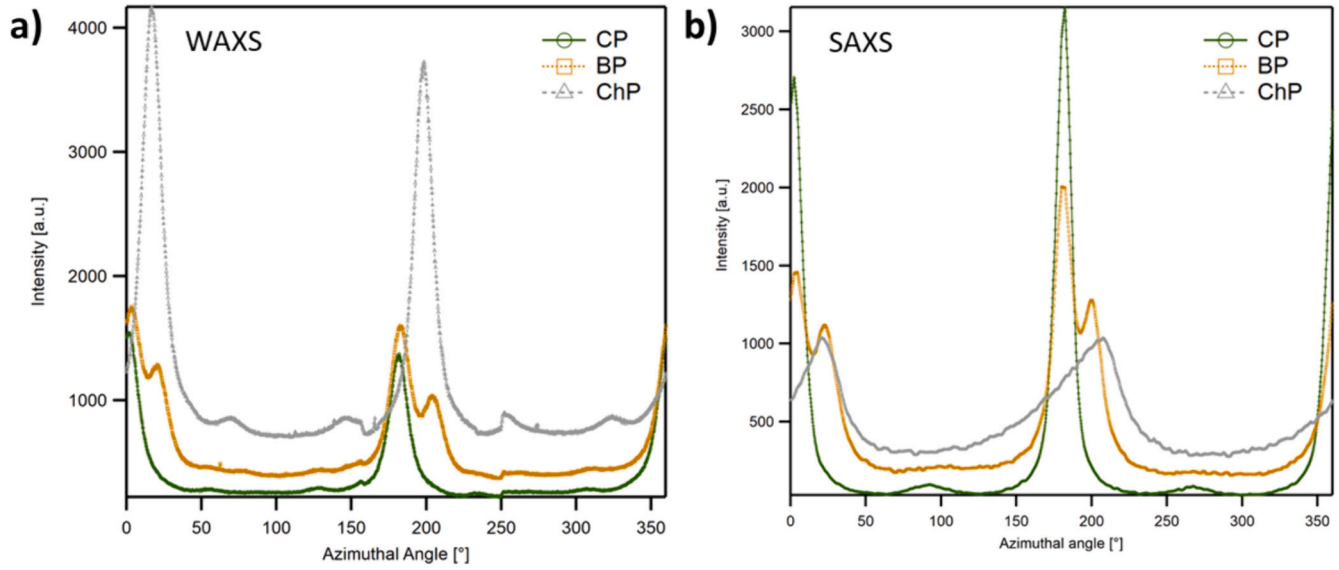

Fig. 3. Effects of the degradation on the microfibril angle distribution. (a) Azimuthal profile from the 200-diffraction peak from the WAXS data. (b) Azimuthal profile from the SAXS data.

Table 6
MFA values obtained from fitting the azimuthal WAXS and SAXS profiles shown in Fig. 3 for intact (CP), biologically degraded (BP) and chemically degraded (ChP) pine wood samples. Values in parentheses correspond to fit uncertainties.

Sample ID	WAXS		SAXS	
	MFA (°)	FWHM (°)	MFA (°)	FWHM (°)
CP	7.2 (0.01)	8.3 (0.03)	7.9 (0.2)	8.35 (0.05)
BP	10.4 (2.4)	14.1 (1.3)	9.5 (0.5)	14.5 (0.13)
ChP	8.4 (2.6)	10.3 (1.9)	18.7 (2.7)	22.8 (1.9)

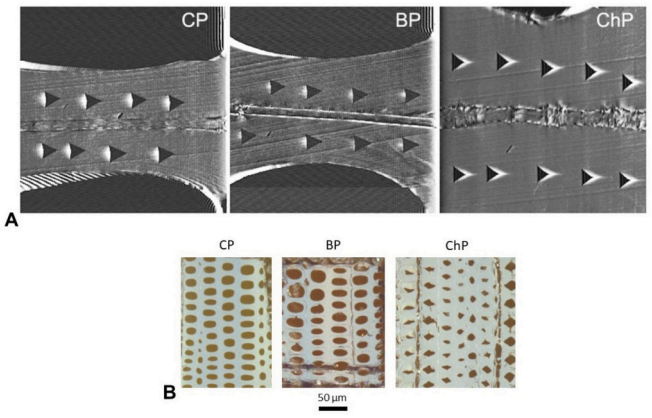

Fig. 4. A - Scanning probe microscopy images of example cross-section morphologies of undegraded (CP), biologically (BP), and chemically (ChP) degraded pinewood after indentation visualizing the thickness of the cell walls; the size of the single image window was 20 × 20 µm; B – microscopy images of undegraded (CP), biologically (BP), and chemically (ChP) degraded pinewood sections prepared for nanoindentation measurements.

4. Discussion and conclusions

The results obtained in the study show differences in wood degraded by brown-rot fungus and alkaline treatment, starting from chemical composition through nanostructure to the macro-scale of the cell wall. By combining our results with previous data on the physical properties of the cell walls, it is evident that the nanoscale changes, particularly at the elementary fibril level, can help understand the differences observed in the moisture and mechanical properties of degraded wood.

The results of the wood chemical analysis obtained in the present research align with the data from our previous FT-IR analysis (Broda, Popescu, et al., 2022) and provide additional support for interpreting nanoscale data. Considering them together with the data from X-ray diffraction (Broda, Popescu, et al., 2022), we can conclude that the decay by *C. puteana* caused loss of cellulose and hemicelluloses (i.e., xylans and mannans) and a decrease in cellulose crystallinity when compared to undegraded wood. Alkaline treatment reduced xylans and soluble lignin content. While NaOH treatment may transform some cellulose I to cellulose II or Na-cellulose, no distinct diffraction peaks from either one of these polymorphs were present in the WAXS data in this study.

The differences observed in the nanostructure due to the degradation methods likely arise from changes imparted to the spatial architecture of the wood polymers in the cell walls, particularly regarding the composition of the cellulose microfibrils and their moisture-accessibility. While the detailed structure of the microfibril is still an active area of research, there is increasing evidence in the literature describing the molecular scale interactions between the wood polymers. Some hemicelluloses have been shown to be in close contact with cellulose (Terrett et al., 2019) and can even occupy some spaces between the elementary fibrils (Thomas et al., 2020). Xylan can also be closely associated with lignin (Kang et al., 2019) and plays a role in microfibril formation and alignment (Crowe et al., 2021). Lignin is generally thought to be part of the microfibril matrix, though there is increasing microscopy-based evidence showing that lignin is required to form microfibrils (Lyczakowski et al., 2019), and it is often found surrounding microfibrils whose size ranges from 5 nm (Kesari et al., 2021) to about 20 to 30 nm (Adobes-Vidal et al., 2020). Hence, microfibrils can be described as a bundle of cellulose elementary fibrils that contain some hemicelluloses (both inside and outside the bundle) and some lignin that is outside this bundle. The differences observed in this study in the elementary fibril spacing indicate that the degradation methods removed wood polymers from the microfibrils and thus affected their moisture-induced swelling. For the chemically degraded sample, we observed the highest increase in elementary fibril spacing both in dry and wet conditions. Previous studies on delignified wood have also shown increased spacing between elementary fibrils (Zhu et al., 2020). The swelling at the elementary fibril level translated to the expansion of the cell wall into the lumen and

the creation of misshapen lumina visible in optical microscopy images of the nanoindentation surface (ChP in Fig. 4B). The increased elementary fibril spacing suggests that as the sample is chemically degraded, there are elementary fibrils that are increasing in size due to the changes in the cellulose crystal lattice by the NaOH treatment, while others may be coalescing due to the extraction of the acid-soluble lignin and/or xylans from the matrix (Table 1). It is also possible that some of the swelling restrictions caused by the presence of lignin/hemicellulose matrix have been released by the treatment. These combined changes give rise to an increased disorder in the microfibril angle of the cellulose microfibrils in the chemically degraded sample compared to the undegraded one.

Exposure to brown rot (*G. trabeum*) has been shown to decrease cellulose crystallinity, as well as increase the size of the elementary fibrils and the spacing between them to allow for further enzymatic degradation (Floudas et al., 2022; Goodell et al., 2017; Plaza et al., 2022; Zhu et al., 2020). For the biologically degraded sample, wood exposure to *C. puteana* targeted both celluloses and hemicelluloses, which led to a slight increase in the elementary fibril cross-section and an increase in the elementary fibril spacing. This latter increase was most noticeable in the wet state, which would indicate that the extensive depletion of hemicelluloses increased the moisture-accessibility of the microfibrils, albeit to a lesser extent compared to the removal of xylan and acid-soluble lignin caused by the chemical treatment (Table 1). It is also possible that the chemical degradation process imparts changes in the cellulose surface and, hence, modifies its interaction with water. Fungal exposure and/or removal of the hemicelluloses can also increase disorder in the arrangement of cellulose microfibrils (Crowe et al., 2021) and lead to higher MFAs (Hudson-McAulay et al., 2018), which is consistent with the higher MFA and less pronounced SANS peak observed for the BP samples. These changes are consistent with a fungal degradation mechanism that lowers the cellulose crystallinity but does not result in "thinning" of the cellulose elementary fibrils, which was previously observed in filter paper degraded by *G. trabeum* (Floudas et al., 2022).

Comparing the nanoscale changes observed in this study to previously measured macroscale physical properties can help us deduce what properties are influenced by the nanostructural changes. From our previous studies on the structure and properties of the degraded wood (Table 7) (Broda et al., 2024; Broda, Popescu, et al., 2022; Broda, Spear, et al., 2022), we know that both degradation processes effectively reduced wood mass loss (the 39 ± 5 % reduction by fungal decay (BP) and 17 ± 1 % by chemical treatment (ChP), and the degraded wood shrunk after air-drying (22.3 % shrinkage for BP and 25.1 % for ChP with regard to undegraded wood (CP)). Despite the degree of degradation, the air-drying caused densification of the decomposed wood so that the final density of BP was similar to CP (0.44 g cm-^{3}), and for ChP, it was even higher (0.65 g cm^{-3}). The changes in the density of the degraded cell walls follow the same trend as the EF_s observed via SANS.

The changes in the chemical composition of wood polymers affected the cell wall microstructure, increasing total pore volume, which is the total volume of pores with diameters from 4 nm to 73 nm measured by nitrogen absorption, and surface area, wherein NaOH treatment produced a greater number of smaller mesopores (with diameters ranging from 4 nm to 11 nm) than fungal decay (Broda, Popescu, et al., 2022). They also affected wood moisture properties – fungal decay reduced the maximum equilibrium moisture content (EMC) measured at about 94 % air relative humidity (RH) from 20.3 % to 17.7 % and did not alter the number of free hydroxy groups compared to undegraded wood while chemical degradation increased the wood maximum EMC to 24.6 % and increased the number of free hydroxy groups from 7.9 mmol g^{-1} to 11.3 mmol g^{-1}. Changes in the EMC of the samples agree with the nanoscale moisture-induced swelling measured via SANS. BP had similar EF_s to undegraded wood but with a lower contrast due to its lower EMC, whereas ChP had both increased EF_s and EMC. Dynamic Mechanical Analysis (DMA) on bulk wood samples revealed a reduction in the loss modulus (E") and storage modulus (E') at the temperature of 25 °C for BP compared to CP, while for ChP, the values were more similar to CP. Both degradation methods increased the damping properties of wood compared to undegraded samples. However, the DMA results were encumbered with errors due to the small internal cracks that occurred in degraded wood samples (hence the higher standard deviation values for those specimens) (Broda, Spear, et al., 2022). Therefore, measurements on the cell wall level were necessary to obtain more precise information about the mechanical properties of the degraded cell walls. For this purpose, we used a nanoindentation technique, which enables measuring the micromechanical properties of the cell walls in sound and degraded wood (Jakes & Stone, 2021; Wimmer et al., 1997).

Table 7
Physical, moisture, and mechanical properties of undegraded (CP), biologically (BP), and chemically (ChP) degraded pinewood. Nanoindentation properties are of the S2 secondary cell wall layer tested on the transverse plane. ± standard deviation.

Property	CP	BP	ChP	Reference
Mass loss (%)	–	38.5 ± 4.7	16.8 ± 1.4	(Broda, Popescu, et al., 2022)
Moisture content during DMA test (%)	6.3 ± 0.1	6.2 ± 0.2	6.9 ± 0.1	(Broda, Spear, et al., 2022)
Shrinkage (%)	–	22.3 ± 4.6	25.1 ± 4.2	(Broda, Popescu, et al., 2022)
Surface area (m^2 g^{-1})	0.36 ± 0.02	0.70 ± 0.06	0.79 ± 0.03	(Broda, Popescu, et al., 2022)
Total pore volume (cm^3 g^{-1})	0.0007	0.0015	0.0012	(Broda, Popescu, et al., 2022)
Cell wall density (g cm-^{3})	1.51 ± 0.002	1.54 ± 0.002	1.57 ± 0.002	(Broda, Popescu, et al., 2022)
Bulk density (g cm^{-3})	0.44 ± 0.02	0.44 ± 0.03	0.65 ± 0.02	(Broda, Popescu, et al., 2022)
Cellulose crystallinity degree (%)	55.9	50.1	52.7	(Broda, Popescu, et al., 2022)
EMC at 94 % RH (%)	19.9	17.1	24.2	(Broda, Spear, et al., 2022)
Hydroxy groups number (mmol g^{-1})	7.90 ± 0.14	8.04 ± 0.99	11.32 ± 0.34	(Broda, Spear, et al., 2022)
DMA E' at 25° (MPa)	95.4 ± 14.1	52.3 ± 10.8	90.8 ± 17.0	(Broda, Spear, et al., 2022)
Nanoindentation elastic modulus (GPa)	16.4 ± 1.8	15.3 ± 1.5	13.8 ± 2.8	(Broda et al., 2024)
Nanoindentation hardness (MPa)	389 ± 26	395 ± 27	358 ± 44	(Broda et al., 2024)

The results obtained from nanoindentation measurements show how the changes in chemistry and nanostructure of the cell walls affect their mechanical properties (Broda et al., 2024). Nanoindentation was used to measure the elastic modulus and hardness of the latewood S2 secondary cell wall in the longitudinal direction. Elastic modulus is a metric of the cell wall's resistance to elastic (recoverable) deformations caused by applied stress. Hardness quantifies the cell wall's resistance to plastic (permanent) deformations. In the longitudinal direction, the elastic modulus will be dominated by the orientation and integrity of the cellulose fibrils (Jäger et al., 2011), whereas hardness is understood to be controlled by yielding in the matrix polymers (Gindl et al., 2004), which consist of lignin, hemicelluloses, and amorphous cellulose. It has been suggested that lignin is the matrix polymer controlling the hardness (Hofstetter et al., 2008). The nanoindentation results (Table 7) and images of prepared surfaces (Fig. 4) provide some additional insights into how the cell walls were degraded. Despite the relatively large mass losses of 17 % and 39 % for ChP and BP, respectively, the changes in measured cell wall properties were modest. Compared to CP, the BP elastic modulus only decreased by 7 %, and the hardness increased by 2 %. For ChP, the elastic modulus decreased by 16 %, and the hardness decreased by 8 %. Furthermore, the integrity of the prepared surfaces

looks similar for CP, BP, and ChP (Fig. 4A). These modest changes in mechanical properties and surface observations could suggest that degradations are not creating large void volumes in the tested cell walls, but rather, the mass loss is likely occurring by the removal of individual polymers, and after removal, the remaining wood polymers are coalescing to reform a structurally sound S2 layer. These ideas are also supported by the increase in elementary fibril spacings shown via SAXS and SANS. The increased cell wall density of the ChP and BP (Table 7) also supports that voids are not being formed in the cell walls and that coalescence of the remaining wood polymers is likely occurring during drying after degradation. It is worth noting that for ChP samples, the standard deviations for the elastic modulus and hardness values were higher than for BP and CP, suggesting a more uneven degradation of this model wood (Broda et al., 2024). Additionally, the BP nanoindentation elastic modulus did not have the drastic decrease like in the storage modulus obtained via DMA (DMA E'). In damaged thin wood sections, Broda et al. observed that BP had much weaker interfaces between the secondary cell walls and middle lamella than in the CP or ChP (Broda et al., 2024). It is likely that the decrease in bulk wood DMA E' arose from this weakened interface rather than a drastic weakening in the cell wall material itself.

There are multiple potential explanations for the differences in nanoindentation properties between CP, BP, and ChP. Elastic modulus and hardness are very sensitive to changes in moisture content, with both hardness and elastic modulus decreasing with increasing moisture (Yu et al., 2011). As previously reported, ChP had a higher max EMC than CP and BP. All nanoindentation experiments were performed under 50 % RH conditions (Broda et al., 2024), where, as reported before (Broda, Spear, et al., 2022), the moisture content (MC) of CP and BP was about 7.5 %, and that of ChP was 10 %. A higher moisture content of ChP can partially explain the lower ChP elastic modulus and hardness. Similarly, BP had the lowest max EMC and moisture content during testing, which likely caused increases in elastic modulus and hardness. Also, given the current understanding that lignin controls hardness (Hofstetter et al., 2008), the degraded lignin in ChP is likely contributing to the lower hardness as compared to CP and BP. Finally, the decreased cellulose crystallinity and increased disorder of the microfibril observed with SANS and SAXS also likely contributed to the lower elastic moduli for ChP and BP as compared to the CP. These results are consistent with previous reports showing that the tensile stiffness of isolated wood fibers was greatly reduced with increasing moisture content as well as increasing MFA (Horbelt et al., 2021).

The results presented herein helped to better understand the structure and properties of model degraded wood material. Applying the two degradation processes caused mass loss, affected the chemical composition, altered the nanostructure, and resulted in modified mechanical properties. Hence, a holistic approach that considers not only the pattern and degree of degradation but also nanoscale changes in the cell wall is crucial from the conservation perspective. By using two different model wood materials for research on new conservation agents, different effects on the wood's dimensional stability can be observed, and a more complete understanding of how new conservation agents interact or restore the cell wall nanostructure can be achieved. While developing a universal conservation agent capable of addressing all types and degrees of wood degradation seems like an extremely challenging task, a better understanding of how the wood structures and properties are affected by degradation can rather help develop treatments tailored to the individual needs of degraded objects.

Classification

Biological Sciences (Applied Physical Sciences/Chemistry/Biophysics and Computational Biology).

Significance statement

Research on new treatments for waterlogged artifacts of wooden cultural heritage requires huge amounts of wood material. Model wood seems well-suited for this purpose, and using it is better than wasting historical wood. Here, we investigated the chemical composition and nanostructure of model wood prepared using two different degradation methods. Chemical and biological degradation impart changes to wood from chemical composition through cell wall nanostructure to mechanical properties. Thus, a more holistic approach to conservation should consider changes across scales. Moreover, our findings suggest that developing strategies tailored to the individual object needs is better than searching for a universal consolidating agent that will suit all cases and purposes.

CRediT authorship contribution statement

Magdalena Broda: Writing – review & editing, Writing – original draft, Visualization, Supervision, Methodology, Investigation, Formal analysis, Conceptualization. **Nayomi Z. Plaza:** Writing – review & editing, Writing – original draft, Visualization, Validation, Software, Methodology, Investigation, Formal analysis, Data curation, Conceptualization. **Joseph E. Jakes:** Writing – review & editing, Writing – original draft, Investigation, Formal analysis. **Carlos Baez:** Writing – review & editing, Investigation. **Sai Venkatesh Pingali:** Writing – review & editing, Resources, Formal analysis, Data curation. **Wim Bras:** Writing – review & editing, Resources, Formal analysis.

Declaration of competing interest

The authors declare that they have no known competing financial interests or personal relationships that could have appeared to influence the work reported in this paper.

Data availability

Data will be made available on request.

Acknowledgments

The research was supported by the Polish-U.S. Fulbright Commission through a Fulbright Senior Award 2020/21 granted to Magdalena Broda. A portion of this work performed acknowledges the support of the Genomic Science Program, Office of Biological and Environmental Research (OBER), U.S. Department of Energy (DOE), under Contract FWP ERKP752. The SANS studies on Bio-SANS were supported by the OBER funded Center for Structural Molecular Biology (CSMB) under Contract FWP ERKP291, using the High Flux Isotope Reactor supported by the Basic Energy Sciences, Department of Energy. Access to the Xeuss 3 SAXS/WAXS instrument was obtained via the ORNL instrumentation pool. The Xeuss 3 instrument was funded via the ORNL LDRD program. Logan Kearney is acknowledged for SAXS data collection support. The findings and conclusions in this publication are those of the authors and should not be construed to represent any official USDA or U.S. Government determination or policy. This manuscript has been coauthored by UT-Battelle, LLC, under Contract No. DE-AC05- 00OR22725 with the U.S. Department of Energy. The United States Government retains and the publisher, by accepting the article for publication, acknowledges that the United States Government retains a non-exclusive, paid-up, irrevocable, worldwide license to publish or reproduce the published form of this manuscript or allow others to do so, for United States Government purposes.

References

Addison, B., Bu, L., Bharadwaj, V., Crowley, M. F., Harman-Ware, A. E., Crowley, M. F., … Ciesielski, P. N. (2024). Atomistic, macromolecular model of the Populus secondary cell wall informed by solid-state NMR. *Science Advances, 10*(1), Article eadi7965. https://doi.org/10.1126/sciadv.adi7965

Adobes-Vidal, M., Frey, M., & Keplinger, T. (2020). Atomic force microscopy imaging of delignified secondary cell walls in liquid conditions facilitates interpretation of wood ultrastructure. *Journal of Structural Biology, 211*(2), Article 107532. https://doi.org/10.1016/j.jsb.2020.107532

Albelda Berenguer, M., Monachon, M., Jacquet, C., Junier, P., Rémazeilles, C., Schofield, E. J., & Joseph, E. (2019). Biological oxidation of sulfur compounds in artificially degraded wood. *International Biodeterioration & Biodegradation, 141*, 62–70. https://doi.org/10.1016/j.ibiod.2018.06.009

Aluri, E. R., Reynaud, C., Bardas, H., Piva, E., Cibin, G., Mosselmans, J. F. W., … Schofield, E. J. (2020). The formation of chemical degraders during the conservation of a wooden Tudor shipwreck. *ChemPlusChem, 85*(8), 1632–1638. https://doi.org/10.1002/cplu.202000160

Arpaci, S. S., Tomak, E. D., Ermeydan, M. A., & Yildirim, I. (2021). Natural weathering of sixteen wood species: Changes on surface properties. *Polymer Degradation and Stability, 183*, Article 109415. https://doi.org/10.1016/j.polymdegradstab.2020.109415

Bagley, S. T., & Richter, D. L. (2002). Biodegradation by brown rot fungi. In H. D. Osiewacz (Ed.), *Industrial applications* (pp. 327–341). Springer. https://doi.org/10.1007/978-3-662-10378-4_16.

Bakri, M. K. B., Jayamani, E., Hamdan, S., Rahman, M. R., Soon, K. H., & Kakar, A. (2016). Fundamental study on the effect of alkaline treatment on natural fibers structures and behaviors. *Journal of Engineering and Applied Sciences, 11*(14), 8759–8763.

Bari, E., Daniel, G., Yilgor, N., Kim, J. S., Tajick-Ghanbary, M. A., Singh, A. P., & Ribera, J. (2020). Comparison of the decay behavior of two white-rot fungi in relation to wood type and exposure conditions. *Microorganisms, 8*(12). https://doi.org/10.3390/microorganisms8121931. Article 12.

Blanchette, R. A. (2000). A review of microbial deterioration found in archaeological wood from different environments. *International Biodeterioration & Biodegradation, 46*(3), 189–204. https://doi.org/10.1016/S0964-8305(00)00077-9

Brischke, C., & Alfredsen, G. (2020). Wood-water relationships and their role for wood susceptibility to fungal decay. *Applied Microbiology and Biotechnology, 104*(9), 3781–3795. https://doi.org/10.1007/s00253-020-10479-1

Brischke, C., Grünwald, L. K., & Bollmus, S. (2020). Effect of size and shape of specimens on the mass loss caused by Coniophora puteana in wood durability tests. *European Journal of Wood and Wood Products, 78*(4), 811–819. https://doi.org/10.1007/s00107-020-01559-0

Brischke, C., Stricker, S., Meyer-Veltrup, L., & Emmerich, L. (2019). Changes in sorption and electrical properties of wood caused by fungal decay. *Holzforschung, 73*(5), 445–455. https://doi.org/10.1515/hf-2018-0171

Broda, M., & Hill, C. A. (2021). Conservation of waterlogged wood—Past, present and future perspectives. *Forests, 12*(9), 1193. https://doi.org/10.3390/f12091193

Broda, M., Jakes, J. E., Li, L., & Antipova, O. A. (2023). Archeological wood conservation with selected organosilicon compounds studied by XFM and nanoindentation. *Wood Science and Technology, 57*, 1277–1298. https://doi.org/10.1007/s00226-023-01503-4

Broda, M., Jakes, J. E., Li, L., Antipova, O. A., Maxey, E. R., & Qiaoling, J. (2024). Conservation of model degraded pine wood with selected organosilicons studied by XFM and nanoindentation. *Wood Science and Technology*. https://doi.org/10.1007/s00226-024-01533-6

Broda, M., Mazela, B., & Dutkiewicz, A. (2019). Organosilicon compounds with various active groups as consolidants for the preservation of waterlogged archaeological wood. *Journal of Cultural Heritage, 35*, 123–128. https://doi.org/10.1016/j.culher.2018.06.006

Broda, M., Mazela, B., & Radka, K. (2019). Methyltrimethoxysilane as a stabilising agent for archaeological waterlogged wood differing in the degree of degradation. *Journal of Cultural Heritage, 35*, 129–139. https://doi.org/10.1016/j.culher.2018.06.004

Broda, M., & Plaza, N. Z. (2023). Durability of model degraded wood treated with organosilicon compounds against fungal decay. *International Biodeterioration & Biodegradation, 178*, Article 105562. https://doi.org/10.1016/j.ibiod.2022.105562

Broda, M., Popescu, C.-M., Curling, S. F., Timpu, D. I., & Ormondroyd, G. A. (2022). Effects of biological and chemical degradation on the properties of scots pine wood—Part I: chemical composition and microstructure of the cell wall. *Materials, 15*(7). https://doi.org/10.3390/ma15072348. Article 7.

Broda, M., Spear, M. J., Curling, S. F., & Dimitriou, A. (2022). Effects of biological and chemical degradation on the properties of scots pine—Part II: wood-moisture relations and viscoelastic behaviour. *Forests, 13*(9). https://doi.org/10.3390/f13091390. Article 9.

Cai, M., Takagi, H., Nakagaito, A. N., Katoh, M., Ueki, T., Waterhouse, G. I., & Li, Y. (2015). Influence of alkali treatment on internal microstructure and tensile properties of abaca fibers. *Industrial Crops and Products, 65*, 27–35. https://doi.org/10.1016/j.indcrop.2014.11.048

Chen, P., Li, Y., Nishiyama, Y., Pingali, S. V., O'Neill, H. M., Zhang, Q., & Berglund, L. A. (2021). Small angle neutron scattering shows nanoscale PMMA distribution in transparent wood biocomposites. *Nano Letters, 21*(7), 2883–2890. https://doi.org/10.1021/acs.nanolett.0c05038

Chen, S. Y., Xue, Z. H., Liu, J. W., Zhao, K. Y., & Bao, X. C. (2018). Effect of alkali treatment on relaxation properties of wood. *Journal of Northwest Forestry University, 33*, 193–197.

Crawshaw, J., Bras, W., Mant, G. R., & Cameron, R. E. (2002). Simultaneous SAXS and WAXS investigations of changes in native cellulose fiber microstructure on swelling in aqueous sodium hydroxide. *Journal of Applied Polymer Science, 83*(6), 1209–1218. https://doi.org/10.1002/app.2287

Crowe, J. D., Hao, P., Pattathil, S., Pan, H., Ding, S.-Y., Hodge, D. B., & Jensen, J. K. (2021). Xylan is critical for proper bundling and alignment of cellulose microfibrils in plant secondary cell walls. *Frontiers in Plant Science, 12*. https://doi.org/10.3389/fpls.2021.737690

Curling, S. F., Clausen, C. A., & Winandy, J. E. (2002). Relationships between mechanical properties, weight loss, and chemical composition of wood during incipient brown-rot decay. *Forest Products Journal, 52*(7/8), 34–39.

Dai, D., & Fan, M. (2014). Wood fibres as reinforcements in natural fibre composites: Structure, properties, processing and applications. In *Natural fibre composites* (pp. 3–65). Elsevier.

Donaldson, L. (2007). Cellulose microfibril aggregates and their size variation with cell wall type. *Wood Science and Technology, 41*(5), 443–460. https://doi.org/10.1007/s00226-006-0121-6

Entwistle, K. M., Eichhorn, S. J., & Navaranjan, N. (2005). The derivation of the cellulose microfibril angle by small-angle X-ray scattering from structurally characterized softwood cell-wall populations. *Journal of Applied Crystallography, 38*(3). https://doi.org/10.1107/S0021889805008319. Article 3.

Fahlén, J., & Salmén, L. (2003). Cross-sectional structure of the secondary wall of wood fibers as affected by processing. *Journal of Materials Science, 38*(1), 119–126. https://doi.org/10.1023/A:1021174118468

Fernando, D., Kowalczyk, M., Guindos, P., Auer, M., & Daniel, G. (2023). Electron tomography unravels new insights into fiber cell wall nanostructure; exploring 3D macromolecular biopolymeric nano-architecture of spruce fiber secondary walls. *Scientific Reports, 13*(1), 2350. https://doi.org/10.1038/s41598-023-29113-x

Floudas, D., Gentile, L., Andersson, E., Kanellopoulos, S. G., Tunlid, A., Persson, P., & Olsson, U. (2022). X-ray scattering reveals two mechanisms of cellulose microfibril degradation by filamentous fungi. *Applied and Environmental Microbiology, 88*(17). https://doi.org/10.1128/aem.00995-22. e00995-22.

Franceschi, E., Cascone, I., & Nole, D. (2008). Study of artificially degraded woods simulating natural ageing of archaeological findings. *Journal of Thermal Analysis and Calorimetry, 92*(1), 319–322. https://doi.org/10.1007/s10973-007-8722-3

Gindl, W., Gupta, H. S., Schöberl, T., Lichtenegger, H. C., & Fratzl, P. (2004). Mechanical properties of spruce wood cell walls by nanoindentation. *Applied Physics A, 79*(8), 2069–2073. https://doi.org/10.1007/s00339-004-2864-y

Goodell, B., Qian, Y., & Jellison, J. (2008). Fungal decay of wood: Soft rot—brown rot—White rot. In *, Vol. 982. Development of commercial wood preservatives* (pp. 9–31). American Chemical Society. https://doi.org/10.1021/bk-2008-0982.ch002.

Goodell, B., Winandy, J. E., & Morrell, J. J. (2020). Fungal degradation of wood: Emerging data, new insights and changing perceptions. *Coatings, 10*(12). https://doi.org/10.3390/coatings10121210. Article 12.

Goodell, B., Zhu, Y., Kim, S., Kafle, K., Eastwood, D., Daniel, G., … O'Neill, H. (2017). Modification of the nanostructure of lignocellulose cell walls via a non-enzymatic lignocellulose deconstruction system in brown rot wood-decay fungi. *Biotechnology for Biofuels, 10*(1), 179. https://doi.org/10.1186/s13068-017-0865-2

Guo, J., Rennhofer, H., Yin, Y., & Lichtenegger, H. C. (2016). The influence of thermo-hygro-mechanical treatment on the micro- and nanoscale architecture of wood cell walls using small- and wide-angle X-ray scattering. *Cellulose, 23*(4), 2325–2340. https://doi.org/10.1007/s10570-016-0982-2

Heller, W. T., Hetrick, J., Bilheux, J., Calvo, J. M. B., Chen, W.-R., DeBeer-Schmitt, L., … Wu, B. (2022). drtsans: The data reduction toolkit for small-angle neutron scattering at Oak Ridge National Laboratory. *SoftwareX, 19*, Article 101101. https://doi.org/10.1016/j.softx.2022.101101

Heller, W. T., Urban, V. S., Lynn, G. W., Weiss, K. L., O'Neill, H. M., Pingali, S. V., … Myles, D. A. (2014). The bio-SANS instrument at the high flux isotope reactor of Oak Ridge National Laboratory. *Journal of Applied Crystallography, 47*(4), 1238–1246. https://doi.org/10.1107/S1600576714011285

N.J. Heyn, A. (1969). The elementary fibril and supermolecular structure of cellulose in soft wood fiber. *Journal of Ultrastructure Research, 26*(1), 52–68. https://doi.org/10.1016/S0022-5320(69)90035-5

Hill, C., Kymäläinen, M., & Rautkari, L. (2022). Review of the use of solid wood as an external cladding material in the built environment. *Journal of Materials Science, 57*, 9031–9076. https://doi.org/10.1007/s10853-022-07211-x

Hofstetter, K., Hellmich, C., Eberhardsteiner, J., & Mang, H. A. (2008). Micromechanical estimates for elastic limit states in wood materials, revealing nanostructural failure mechanisms. *Mechanics of Advanced Materials and Structures, 15*(6–7), 474–484. https://doi.org/10.1080/15376490802142387

Horbelt, N., Dunlop, J. W. C., Bertinetti, L., Fratzl, P., & Eder, M. (2021). Effects of moisture and cellulose fibril angle on the tensile properties of native single Norway spruce wood fibres. *Wood Science and Technology, 55*(5), 1305–1318. https://doi.org/10.1007/s00226-021-01315-4

Hudson-McAulay, K., Auty, D., & Jarvis, M. C. (2018). FTIR measurement of cellulose microfibril angle in historic scots pine wood and its use to detect fungal decay. *Studies in Conservation, 63*(6), 375–382. https://doi.org/10.1080/00393630.2017.1353282

Ibach, R. E., Plaza, N. Z., & Pingali, S. V. (2022). Small angle neutron scattering reveals wood nanostructural features in decay resistant chemically modified wood. *Frontiers in Forests and Global Change Journal, 4*, 1–11. https://doi.org/10.3389/ffgc.2021.814086

Ilavsky, J. (2012). Nika: Software for two-dimensional data reduction. *Journal of Applied Crystallography, 45*(2). https://doi.org/10.1107/S0021889812004037. Article 2.

Ilavsky, J., & Jemian, P. R. (2009). Irena: Tool suite for modeling and analysis of small-angle scattering. *Journal of Applied Crystallography, 42*(2). https://doi.org/10.1107/S0021889809002222. Article 2.

Ishikura, Y., Abe, K., & Yano, H. (2010). Bending properties and cell wall structure of alkali-treated wood. *Cellulose, 17*(1), 47–55. https://doi.org/10.1007/s10570-009-9360-7

Ishikura, Y., & Nakano, T. (2005). Adsorption properties and structural features of alkali treated wood. *Journal of the Japan Wood Research Society (Japan), 51*(6), 364–371.

Ishikura, Y., & Nakano, T. (2007). Contraction of the microfibrils of wood treated with aqueous NaOH: Evidence from changes in the anisotropy of the longitudinal and transverse swelling rates of wood. *Journal of Wood Science, 53*(2). https://doi.org/10.1007/s10086-006-0870-8. Article 2.

Jäger, A., Hofstetter, K., Buksnowitz, C., Gindl-Altmutter, W., & Konnerth, J. (2011). Identification of stiffness tensor components of wood cell walls by means of nanoindentation. *Composites Part A: Applied Science and Manufacturing, 42*(12), 2101–2109. https://doi.org/10.1016/j.compositesa.2011.09.020

Jakes, J. E., & Stone, D. S. (2021). Best practices for quasistatic Berkovich nanoindentation of wood cell walls. *Forests, 12*(12). https://doi.org/10.3390/f12121696. Article 12.

Jakob, H. F., Fengel, D., Tschegg, S. E., & Fratzl, P. (1995). The elementary cellulose fibril in Picea abies: Comparison of transmission electron microscopy, small-angle X-ray scattering, and wide-angle X-ray scattering results. *Macromolecules, 28*(26), 8782–8787. https://doi.org/10.1021/ma00130a010

Kang, X., Kirui, A., Dickwella Widanage, M. C., Mentink-Vigier, F., Cosgrove, D. J., & Wang, T. (2019). Lignin-polysaccharide interactions in plant secondary cell walls revealed by solid-state NMR. *Nature Communications, 10*(1). https://doi.org/10.1038/s41467-018-08252-0. Article 1.

Kennedy, A., & Pennington, E. R. (2014). Conservation of chemically degraded waterlogged wood with sugars. *Studies in Conservation, 59*(3), 194–201. https://doi.org/10.1179/2047058413Y.0000000109

Kesari, K. K., O'Reilly, P., Seitsonen, J., Ruokolainen, J., & Vuorinen, T. (2021). Infrared photo-induced force microscopy unveils nanoscale features of Norway spruce fibre wall. *Cellulose, 28*(11), 7295–7309. https://doi.org/10.1007/s10570-021-04006-2

Kirui, A., Zhao, W., Deligey, F., Yang, H., Kang, X., Mentink-Vigier, F., & Wang, T. (2022). Carbohydrate-aromatic interface and molecular architecture of lignocellulose. *Nature Communications, 13*(1), 538. https://doi.org/10.1038/s41467-022-28165-3

Knudsen, E. B., Sørensen, H. O., Wright, J. P., Goret, G., & Kieffer, J. (2013). FabIO: Easy access to two-dimensional X-ray detector images in Python. *Journal of Applied Crystallography, 46*(2), 537–539. https://doi.org/10.1107/S0021889813000150

Larocque, G. L., & Maass, O. (1941). The mechanism of the alkaline delignification of wood. *Canadian Journal of Research, 19*(1), 1–16. https://doi.org/10.1139/cjr41b-001

Li, G.-Y., Huang, L.-H., Hse, C.-Y., & Qin, T.-F. (2011). Chemical compositions, infrared spectroscopy, and X-ray diffractometry study on brown-rotted woods. *Carbohydrate Polymers, 85*(3), 560–564. https://doi.org/10.1016/j.carbpol.2011.03.014

Lichtenegger, H., Reiterer, A., Stanzl-Tschegg, S. E., & Fratzl, P. (1999). Variation of cellulose microfibril angles in softwoods and hardwoods—A possible strategy of mechanical optimization. *Journal of Structural Biology, 128*(3), 257–269. https://doi.org/10.1006/jsbi.1999.4194

Lichtenegger, H. C., Reiterer, A., Stanzl-Tschegg, S. E., & Fratzl, P. (2001). Comment about "the measurement of the micro-fibril angle in soft-wood" by K. M. Entwistle and N. J. Terrill. *Journal of Materials Science Letters, 20*(24), 2245–2247. https://doi.org/10.1023/A:1017957606391

Liu, L., Zhang, L., Zhang, B., & Hu, Y. (2019). A comparative study of reinforcement materials for waterlogged wood relics in laboratory. *Journal of Cultural Heritage, 36*, 94–102. https://doi.org/10.1016/j.culher.2018.08.002

Lyczakowski, J. J., Bourdon, M., Terrett, O. M., Helariutta, Y., Wightman, R., & Dupree, P. (2019). Structural imaging of native cryo-preserved secondary cell walls reveals the presence of macrofibrils and their formation requires normal cellulose, lignin and xylan biosynthesis. *Frontiers in Plant Science, 10*, 1398. https://doi.org/10.3389/fpls.2019.01398

Martínez-Sanz, M., Gidley, M. J., & Gilbert, E. P. (2015). Application of X-ray and neutron small angle scattering techniques to study the hierarchical structure of plant cell walls: A review. *Carbohydrate Polymers, 125*, 120–134. https://doi.org/10.1016/j.carbpol.2015.02.010

Monaco, A. L., Balletti, F., & Pelosi, C. (2018). Wood in cultural heritage. Properties and conservation of historical wooden artefacts. *European Journal of Science and Theology, 14*, 161–171.

Nishimura, H., Okano, T., & Sarko, A. (1991). Mercerization of cellulose. 5. Crystal and molecular structure of Na-cellulose I. *Macromolecules, 24*(3), 759–770. https://doi.org/10.1021/ma00003a020

Nishiyama, Y., Kuga, S., & Okano, T. (2000). Mechanism of mercerization revealed by X-ray diffraction. *Journal of Wood Science, 46*(6), 452–457. https://doi.org/10.1007/BF00765803

Pandey, K. K., & Pitman, A. J. (2003). FTIR studies of the changes in wood chemistry following decay by brown-rot and white-rot fungi. *International Biodeterioration & Biodegradation, 52*(3), 151–160. https://doi.org/10.1016/S0964-8305(03)00052-0

Penttilä, P. A., Altgen, M., Awais, M., Österberg, M., Rautkari, L., & Schweins, R. (2020). Bundling of cellulose microfibrils in native and polyethylene glycol-containing wood cell walls revealed by small-angle neutron scattering. *Scientific Reports, 10*(1), 1–9. https://doi.org/10.1038/s41598-020-77755-y

Penttilä, P. A., Altgen, M., Carl, N., van der Linden, P., Morfin, I., Österberg, M., … Rautkari, L. (2020). Moisture-related changes in the nanostructure of woods studied with X-ray and neutron scattering. *Cellulose, 27*(1), 71–87. https://doi.org/10.1007/s10570-019-02781-7

Penttilä, P. A., Rautkari, L., Österberg, M., & Schweins, R. (2019). Small-angle scattering model for efficient characterization of wood nanostructure and moisture behaviour. *Journal of Applied Crystallography, 52*(2), 369–377. https://doi.org/10.1107/S1600576719002012

Penttilä, P. A., Zitting, A., Lourençon, T., Altgen, M., Schweins, R., & Rautkari, L. (2021). Water-accessibility of interfibrillar spaces in spruce wood cell walls. *Cellulose, 28*(18), 11231–11245. https://doi.org/10.1007/s10570-021-04253-3

Plaza, N. Z., Jakes, J. E., Frihart, C. R., Hunt, C. G., Yelle, D. J., Lorenz, L. F., … Stone, D. S. (2018). Small-angle neutron scattering as a new tool to evaluate moisture-induced swelling in the nanostructure of chemically modified wood cell walls*. *Forest Products Journal, 68*(4), 349–352. https://doi.org/10.13073/FPJ-D-17-00065

Plaza, N. Z., Pingali, S. V., & Ibach, R. E. (2022). Nanostructural changes correlated to decay resistance of chemically modified wood fibers. *Fibers, 10*(5). https://doi.org/10.3390/fib10050040. Article 5.

Plaza, N. Z., Pingali, S. V., Qian, S., Heller, W. T., & Jakes, J. E. (2016). Informing the improvement of forest products durability using small angle neutron scattering. *Cellulose, 23*(3), 1593–1607. https://doi.org/10.1007/s10570-016-0933-y

Pournou, A. (2020a). Wood deterioration by aquatic microorganisms. In A. Pournou (Ed.), *Biodeterioration of wooden cultural heritage: Organisms and decay mechanisms in aquatic and terrestrial ecosystems* (pp. 177–260). Springer International Publishing. https://doi.org/10.1007/978-3-030-46504-9_4.

Pournou, A. (2020b). Wood deterioration by terrestrial microorganisms. In *Biodeterioration of wooden cultural heritage* (pp. 345–424). Springer.

Raia, R. Z., Iwakiri, S., Trianoski, R., Andrade, A. S.d., & Kowalski, E. L. (2021). Effects of alkali treatment on modification of the Pinus fibers. *Matéria (Rio de Janeiro), 26*. https://doi.org/10.1590/S1517-707620210001.1236

Ringman, R., Pilgård, A., Brischke, C., & Richter, K. (2014). Mode of action of brown rot decay resistance in modified wood: A review. *Holzforschung, 68*(2), 239–246. https://doi.org/10.1515/hf-2013-0057

Rowell, R. M., Ibach, R. E., McSweeny, J., & Nilsson, T. (2009). Understanding decay resistance, dimensional stability and strength changes in heat-treated and acetylated wood. *Wood Material Science & Engineering, 4*(1–2), 14–22. https://doi.org/10.1080/17480270903261339

Saiful Islam, M., Hamdan, S., Jusoh, I., Rezaur Rahman, M., & Ahmed, A. S. (2012). The effect of alkali pretreatment on mechanical and morphological properties of tropical wood polymer composites. *Materials & Design, 33*, 419–424. https://doi.org/10.1016/j.matdes.2011.04.044

Sandberg, D., Kutnar, A., & Mantanis, G. (2017). Wood modification technologies—A review. *iForest - Biogeosciences and Forestry, 10*(6), 895. https://doi.org/10.3832/ifor2380-010

Sluiter, A., Hames, B., Ruiz, R., Scarlata, C., Sluiter, J., Templeton, D., & Crocker, D. (2008). Determination of structural carbohydrates and lignin in biomass. *National Renewable Energy Laboratory - Technical Report, 1617*(1), 1–16.

Spear, M. J., Curling, S. F., Dimitriou, A., & Ormondroyd, G. A. (2021). Review of functional treatments for modified wood. *Coatings, 11*(3). https://doi.org/10.3390/coatings11030327. Article 3.

Tahira, A., Howard, W., Pennington, E. R., & Kennedy, A. (2017). Mechanical strength studies on degraded waterlogged wood treated with sugars. *Studies in Conservation, 62*(4), 223–228. https://doi.org/10.1080/00393630.2016.1169364

Terrett, O. M., Lyczakowski, J. J., Yu, L., Iuga, D., Franks, W. T., Brown, S. P., … Dupree, P. (2019). Molecular architecture of softwood revealed by solid-state NMR. *Nature Communications, 10*(1). https://doi.org/10.1038/s41467-019-12979-9. Article 1.

Thomas, L. H., Martel, A., Grillo, I., & Jarvis, M. C. (2020). Hemicellulose binding and the spacing of cellulose microfibrils in spruce wood. *Cellulose, 27*(8), 4249–4254. https://doi.org/10.1007/s10570-020-03091-z

Toba, K., Yamamoto, H., & Yoshida, M. (2013). Crystallization of cellulose microfibrils in wood cell wall by repeated dry-and-wet treatment, using X-ray diffraction technique. *Cellulose, 20*(2), 633–643. https://doi.org/10.1007/s10570-012-9853-7

Wakefield, J. M. K., Braovac, S., Kutzke, H., Stockman, R. A., & Harding, S. E. (2020). Tert-butyldimethylsilyl chitosan synthesis and characterization by analytical ultracentrifugation, for archaeological wood conservation. *European Biophysics Journal, 49*(8), 781–789. https://doi.org/10.1007/s00249-020-01450-z

Wei, T. S., Geng, B. J., Qi, L. H., Tiong, G. K., Chi, K. S., & Hoong, W. W. (2018). Effect of bleaching using sodium hydroxide on pulp derived from Sesbania grandiflora. *Journal of Tropical Resources and Sustainable Science (JTRSS), 6*(1), 1–3. https://doi.org/10.47253/jtrss.v6i1.718

Wimmer, R., Lucas, B. N., Oliver, W. C., & Tsui, T. Y. (1997). Longitudinal hardness and Young's modulus of spruce tracheid secondary walls using nanoindentation technique. *Wood Science and Technology, 31*(2), 131–141. https://doi.org/10.1007/BF00705928

Xu, E., Wang, D., & Lin, L. (2020). Chemical structure and mechanical properties of wood cell walls treated with acid and alkali solution. *Forests, 11*(1), 87. https://doi.org/10.3390/f11010087

Xu, P., Donaldson, L. A., Gergely, Z. R., & Staehelin, L. A. (2007). Dual-axis electron tomography: A new approach for investigating the spatial organization of wood cellulose microfibrils. *Wood Science and Technology, 41*(2), 101–116. https://doi.org/10.1007/s00226-006-0088-3

Yu, Y., Fei, B., Wang, H., & Tian, G. (2011). Longitudinal mechanical properties of cell wall of Masson pine (Pinus massoniana Lamb) as related to moisture content: A nanoindentation study. *Holzforschung, 65*(1), 121–126. https://doi.org/10.1515/hf.2011.014

Zabel, R. A., & Morrell, J. J. (2020). Chapter eight—Chemical changes in wood caused by decay fungi. In R. A. Zabel, & J. J. Morrell (Eds.), *Wood microbiology* (2nd ed., pp. 215–244). Academic Press. https://doi.org/10.1016/B978-0-12-819465-2.00008-5.

Zhang, Y. Z., Chen, X. L., Liu, J., Gao, P. J., Shi, D. X., & Pang, S. J. (1997). Size and arrangement of elementary fibrils in crystalline cellulose studied with scanning tunneling microscopy. *Journal of Vacuum Science & Technology, B: Microelectronics and Nanometer Structures–Processing, Measurement, and Phenomena, 15*(4), 1502–1505. https://doi.org/10.1116/1.589483

Zhu, Y., Plaza, N., Kojima, Y., Yoshida, M., Zhang, J., Jellison, J., … Goodell, B. (2020). Nanostructural analysis of enzymatic and non-enzymatic brown rot fungal deconstruction of the lignocellulose cell wall. *Frontiers in Microbiology, 11*, 1389. https://doi.org/10.3389/fmicb.2020.01389

Zisi, A. (2021). Forest wood through the eyes of a cultural conservator. *Forests, 12*(8). https://doi.org/10.3390/f12081001. Article 8.

Zitting, A., Paajanen, A., Rautkari, L., & Penttilä, P. A. (2021). Deswelling of microfibril bundles in drying wood studied by small-angle neutron scattering and molecular dynamics. *Cellulose, 28*(17), 10765–10776. https://doi.org/10.1007/s10570-021-04204-y